Journal of ELECTRONIC MATERIALS, Vol. 49, No. 1, 2020
https://doi.org/10.1007/s11664-019-07681-x

Thermal, Electrical and Mechanical Properties of Expanded Graphite and Micro-SiC Filled Hybrid Epoxy Composite for Electronic Packaging Applications

SAGAR KUMAR NAYAK ,[1,2] SMITA MOHANTY,[1] and SANJAY K. NAYAK[1]

1.—SARP-Laboratory for Advanced Research in Polymeric Materials (LARPM), Central Institute of Plastics Engineering and Technology (CIPET), B-25, CNI Complex, Patia, Bhubaneswar, Odisha 751024, India. 2.—e-mail: nayak.sagarkumar@yahoo.in

The synthesis of high-thermal-conductivity expanded graphite (EG) by a physical method from natural graphite flakes using zinc nitrate hexahydrate is described herein. This article establishes thermal conductivity studies of the epoxy composite system containing a hybrid of EG, a soft material, and micro-SiC, a hard material, with different filler fractions. To verify the texture and appearance, the filler materials were characterized by polarized light and scanning electron microscopy. The thermal conductivity of the fabricated hybrid epoxy composites was analyzed by a guarded hot plate meter technique. The electrical properties of the hybrid composite were evaluated by a four-point potentiometer. The single-lap shear strength of optimized composition was observed under a universal testing machine. The thermomechanical behavior and thermal stability of the hybrid composites were investigated through dynamic mechanical analysis and thermogravimetric analysis, respectively. The dispersive status and synergistic effect of the hybrid filler inside the epoxy matrix were studied through fracture surface analysis by scanning electron microscopy. With the addition of 15 wt.% EG and 15 wt.% micro-SiC to the epoxy resin, thermal conductivity of up to 2.24 W/mK was achieved for the hybrid composite, which was an 11.6-fold improvement over unaided epoxy.

Key words: Thermal conductivity, electrical conductivity, expanded graphite, silicon carbide (SiC), epoxy, hybrid composites

INTRODUCTION

Thermally conductive composites have established their suitability for high-power-density microelectronic chips as gap filling materials, heat spreaders, thermal pastes, and pads. A crucial application is as thermal interface materials (TIMs), which ensure good thermal interaction between the chip (source) and the metallic sink to protect electronic components from thermal shock, as heat accumulation affects the performance, life span and reliability of high-efficiency, multifunctional electronic devices.[1,2] In addition to thermal conductivity, the packaging materials must possess properties including low coefficient of thermal expansion, low dielectric properties, low moisture absorption, and thermal and chemical resistance.[3] Epoxy resin is an excellent organic matrix with attractive mechanical and tribological properties, and thermal and chemical stability. Epoxy-based materials are also known for their cryogenic applications in coatings, fuel tanks, and aerospace industry[4] They show high electrical insulating and

(Received April 12, 2019; accepted September 25, 2019; published online October 22, 2019)

very low thermal conducting (~ 0.192 W/mK) properties. To achieve the desired properties of epoxy-based TIMs, the epoxy resin, due to its compatibility with various materials, is usually blended with very high intrinsic thermally conductive filler for the manifestation of improved parameters.[5] Among various thermally conductive fillers, including ceramic, metallic and carbon fillers, expanded graphite (EG) has excellent thermal conductivity (100 W/mK), low density, and excellent mechanical properties, with very convenient preparation for large-scale applications, as compared with graphene, graphene oxide (GO) and CNTs.[3,6,7] Thermal conductivity along with electrical insulation are the key parameters of TIMs. To satisfy this criteria, silicon carbide (SiC), a hard ceramic material displaying high thermal conductivity (~ 270 W/mK) and low coefficient of thermal expansion, is incorporated into the epoxy matrix.[5,8] Generally, SiC is prepared by an Acheson process in which a mixture of petroleum coke and silica or quartz sand in an electrical resistance furnace is reacted chemically at a high-temperature range of 1700–2500°C.[9,10] The SiC is also utilized to fabricate the electromagnetic interference (EMI)-shielding materials, as described by various researchers. A SiC matrix reinforced with SiC fiber as ceramic matrix composite containing different thicknesses of pyrolytic carbon interphase was prepared by chemical vapor infiltration (CVI) and precursor infiltration pyrolysis (PIP) for prospective EMI shielding application in the frequency range of 8.2–12.4 GHz,[11,12] with 25 dB shielding efficiency. Mei et al.[13] fabricated a carbon fiber (CF)-reinforced SiC composite by attaching CNT on the CF surface through electrophoretic deposition (EPD) followed by densification through CVI, and reported a maximum 38.2 dB of EMI absorption shielding efficiency.

In this work, EG is embedded with micro-SiC to develop a hybrid filler for amplification of thermal conductivity of the epoxy composite. Accordingly, EG is synthesized by a simple physical method, and coarse micro-SiC is hybridized with EG to improve the thermal conductivity and also to retain the electrical resistivity of the epoxy.

Srinivas et al. established the synergistic effect of graphite and SiC powder inside the epoxy matrix with a thermal conductivity improvement of 0.71 W/mK at 20 wt.% for each filler loading. They also verified using numerical models including Maxwell, Nielsen, Hashin, and Cheng-Vachon and reported that the experimental values and theoretical values were nearly identical.[5] In the study by Wang et al., 4.5 wt.% silane-modified EG epoxy composite showed thermal conductivity of 1.0 W/mK, which was greater than the unmodified EG loading in the epoxy matrix at an equivalent weight fraction.[3] Zhou et al. found that at 5 wt.% silane-treated carboxyl-functionalized multi-walled CNTs (MWCNTs) and 55 wt.% oxidized and silane-functionalized micro-SiC, the thermal conductivity of the epoxy hybrid composite was approximately 6.7 W/mK. Their results are attributed to the synergistic contribution of micro- and nanofillers.[14] Mun et al. prepared a hybrid filler using a simple sol–gel method by taking polyvinylpyrrolidone (PVP)-treated EG, which was coated with a ceramic casing (SiO_2 or BN/SiO_2). They optimized a thermally conducting composite at a filler fraction of 30 wt.% BN/SiO_2/EG-BN by considering surface resistivity and breakdown strength. They also reported that at 60 wt.% loading of neat EG inside the matrix, the thermal conductivity increased to 11.7 W/mK.[6]

In order to achieve a heat-conducting path through the percolation threshold network and to develop an epoxy with high thermal conductivity as TIM, very high filler loading is usually considered. In the analysis of high filler content, i.e. more than 60 wt.%, the thermal conductivity value increases; however, poor mechanical properties and high density negatively affect the prospective end application. Generally, the range of thermal conductivity of epoxy composites is controlled by conductive filler content and filler morphology. In this investigation, the filler content is optimized to maximize the mechanical and thermal properties for practical use.[14,15] The strategy for the design of more thermally conductive networks is described as high-performance TIMs.

EXPERIMENTAL

Raw Materials

Natural graphite flakes (NGFs) were obtained from Sigma Aldrich. Zinc nitrate hexahydrate was supplied by Sisco Research Laboratories Pvt. Ltd. (India). The micro-SiC powder (purity ~ 90%) was procured from Nanoshel Intelligent Materials (India), with an average particle size of 10–15 μm. The epoxy resin (Araldite GY 250) and cross-linking agent tri-ethylene tetra amine (TETA) were provided by M/S Huntsman International Pvt. Ltd., India.

Production of Expanded Graphite (EG)

The mechanical mixing of natural graphite flakes (NGFs) with crystalline zinc nitrate hexahydrate (ZNHH) [$Zn(NO_3)_2{\cdot}6H_2O$], an oxidizing foaming agent, was carried out. A 1:4 ratio of NGFs and ZNHH was mixed with a cryomill without the ball and liquid nitrogen for 2 min at a frequency of 20 Hz. Then the whole mixture was kept in a muffle furnace at 900°C for 4 min for thermal shock followed by air cooling. The expansion of NGFs has the appearance of interconnected carbon foam with a worm-like whitish appearance as shown in Fig. 1. The expansion volume of EG was analyzed by the measuring cylinder with respect to NGF by pouring 2 g each (Fig. 2).

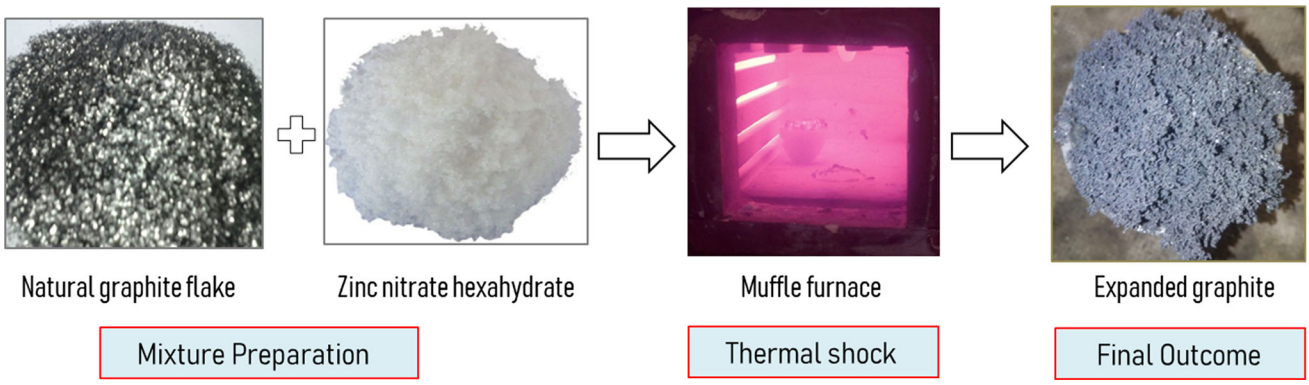

Fig. 1. Schematic illustration of EG synthesis.

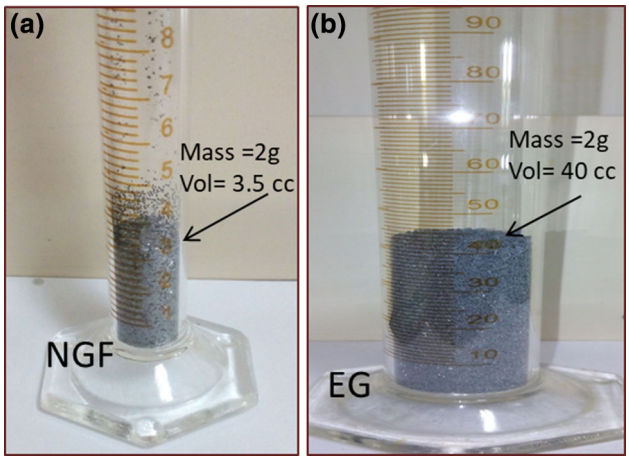

Fig. 2. Expansion analysis of (a) NGFs and (b) EG considering 2g each.

Fabrication of Epoxy Hybrid Composites

Initially, 5 wt.%, 10 wt.% and 15 wt.% EG samples were dehydrated in a vacuum oven at 80°C for 1 h to eliminate the moisture. A predefined amount of epoxy resin was dried in three different containers using a vacuum oven at 70°C for 1 h for bubble removal and viscosity reduction, as the fabrication process was solvent-less. This was followed by hand mixing of EG and epoxy for 15 min, followed by mechanical stirring for 1 h. The cross-linking agent TETA was then mixed (at a ratio of 1:10) with the epoxy, followed by 10 min of vacuum pumping to remove micro-bubbles. The prepared composite was then poured into a mould, and a 5-kg load was applied for compaction of filler to avoid void formation, and was subsequently left for 24 h at room temperature for curing. Similarly, micro-SiC of 5 wt.%, 10 wt.% and 15 wt.% was mechanically mixed with the same amount of EG via cryomilling (without the ball and liquid nitrogen at 20 Hz frequency) for 2 min. Then, 10 wt.%, 20 wt.% and 30 wt.% of the hybrid filler of EG-micro-SiC with equal weights were incorporated separately in low-viscosity epoxy followed by 1 h agitation of each hybrid composite, and a hardener was added in a certain ratio as defined earlier followed by 5 min stirring and vacuum pumping. The three different hybrid composites were then poured into a mould with the same load application. In this approach, six different composites (each composition three samples) were prepared as described in Table I.

Characterization and Measurement

X-ray diffraction (Shimadzu, XRD-7000L, Japan) was used to study the crystal structure of synthesized EG, and the morphology was investigated by transmission electron microscopy (TEM; JEOl JEM 1400). EDAX/SEM was used for microanalysis of EG. The synthesized EG and adopted micro-SiC surfaces were studied using polarized light microscopy and scanning electron microscopy (SEM, Carl Zeiss SMT, Germany). Steady-state through-plane thermal conductivity (TC) of the composites was measured using a Unitherm 2022 guarded heat flow meter (Anter Corp, USA) following ASTM E1530-6 as per Eq. 1.

$$Q = \frac{T_1 - T_2}{L/KA} \tag{1}$$

where Q = rate of heat flow (J/s), L = thickness of the sample (m), K = thermal conductivity (W/mK), A = unit area perpendicular to the heat flow.

Measurement of electrical resistance was carried out by a four-point potentiometric method at a constant voltage. The dimensions of the sample used to study the electrical conductivity were 50 × 50 × 2.5 mm. The four-point probe is scanned in steps over the sample surface; with each scanning step, the voltage–current ratio is evaluated. Lap shear strength of the epoxy composite system was determined using tensile testing with a universal testing machine (UTM) as per ASTM D1002 by the crosshead pull of 0.05 inch/min. The lap shear specimen was prepared by joining two mechanically polished aluminum substrates by adhesive composite referred to as a single lap joint. The presented data are the average of at least three measurements. To determine storage modulus (E'), loss

Table I. Composition of fabricated composite with sample code

Sample no.	Sample code	Total filler (wt.%)	EG (wt.%)	SiC (wt.%)	Epoxy matrix (wt.%)
1	Neat epoxy (Ep)	0	0	0	100
2	EG5-Ep	5	5	0	95
3	EG5-S5-Ep	10	5	5	90
4	EG10-Ep	10	10	0	90
5	EG10-S10-Ep	20	10	10	80
6	EG15-Ep	15	15	0	85
7	EG15-S15-Ep	30	15	15	70

modulus (E''), loss factor (tan δ) and glass transition temperature (T_g) of neat epoxy and its composite system at different filler concentrations, dynamic mechanical analysis (DMA Q800, TA Instruments, USA) was performed as per ASTM D5026. The prepared rectangular samples (65 mm × 12.76 mm × 3.12 mm) were tested using double-cantilever mode with 1 Hz frequency (corresponding to a strain rate of 0.05% per second) along with the heating rate of 10°C/min. DMA was recorded at a temperature scan range of 30–200°C. To verify thermal stability, thermogravimetric analysis (TGA; Q50, TA Instruments, USA) was carried out following the ASTM E1868 standard. The samples were heated from room temperature to 600°C at a heating rate of 10°C/min under a nitrogen purging rate of 60 mL/min. SEM was operated to visualize the fracture surface morphology of optimized composition.

RESULTS AND DISCUSSION

Figure 3 demonstrates the XRD patterns of EG synthesized from thermal treatment with ZNHH [$Zn(NO_3)_2{\cdot}6H_2O$]. The crystalline structure of EG is visible from the two heightened peaks at 2θ = 26.52° (002) and 54.64° (004).[16] An extra peak at 2θ = 44.16° was detected at the (101) plane, confirming the carbon sample, according to Wang et al.[17] As per Bragg's relation $n\lambda = 2d\sin\theta$ (d = interplanar spacing of graphitic plane), at 26.52° and 54.64° diffraction angles, the corresponding d spacing is 0.3357 nm and 0.1677 nm. The peaks at 2θ = 31.8°, 34.24°, 36.1°, 47.62°, 56.5°, 62.84°, 64.91° and 67.9° correspond to (100), (002), (101), (102), (110), (103), (200) and (112) of ZnO nanoparticles. As per zincite, (JCPDS 5-0664), ZnO has a polycrystalline wurtzite structure. The average crystallite size (d_P) of ZnO nanoparticles was estimated using Scherrer's formula (Eq. 2).

$$d_P = \frac{k\lambda}{\beta\cos\theta} \tag{2}$$

where k = shape factor (0.9) and λ = X-ray wavelength of CuKα radiation, i.e. 1.54 Å. θ = Braggs diffraction angle and β is the full width at half maximum (FWHM) of the relevant diffraction peak in radian. From XRD data, the average crystallite size was found to be 34.98 ± 12.23 nm,[18] which is also evident from the TEM image (Fig. 4). The red dotted arrow represents the graphene layers and the white arrow the ZnO traces.

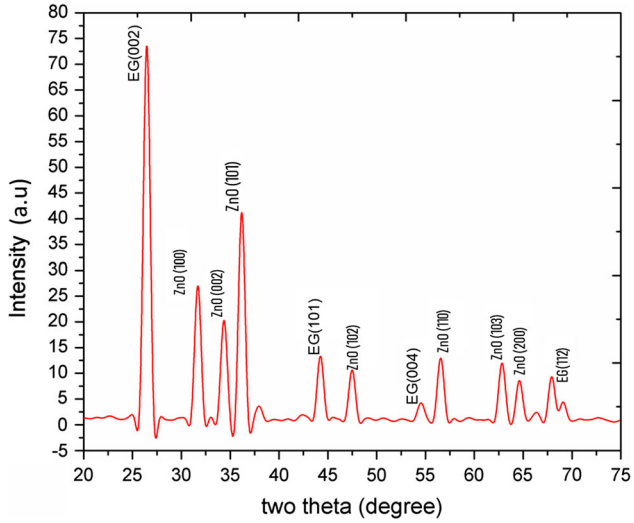

Fig. 3. XRD patterns of expanded graphite (EG).

As zinc nitrate experiences thermal treatment with NGF and becomes an intercalating agent, it creates zinc oxide (ZnO), as described in Eq. 3, which remains attached to the EG surface, as confirmed from XRD analysis.

$$2Zn(NO_3)_2 \rightarrow 2ZnO + 4NO_2 + O_2 \tag{3}$$

The deposition of ZnO nanoparticles on EG substrates is confirmed from SEM/EDAX analysis as shown in Fig. 5, and the carbon remains as the principal element of the synthesized EG, which is also evident from Fig. 5. The inset illustrates the compositional analysis in mass (wt.%) and atomic (at.%) percentage. Because of the limitations of the material in specific analytical conditions, the values presented are approximate.[19]

Figure 6a and b represents the optical and SEM images of procured SiC powder. SiC is characterized by sharp-edged particles with an uneven coarse appearance. The crystal structure of SiC is a zinc blend type with a coordination number of 4. After thermal treatment of NGFs with ZNHH, the optical and SEM images of synthesized EG are shown in

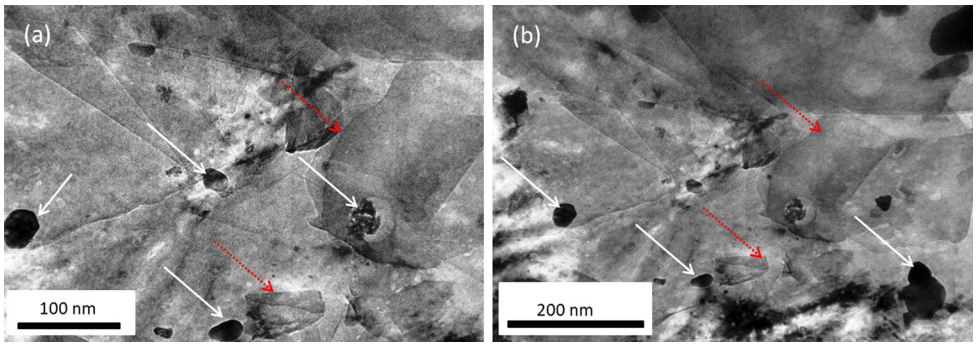

Fig. 4. TEM image of EG containing ZnO nanoparticles at (a) 100 nm scale and (b) 200 nm scale.

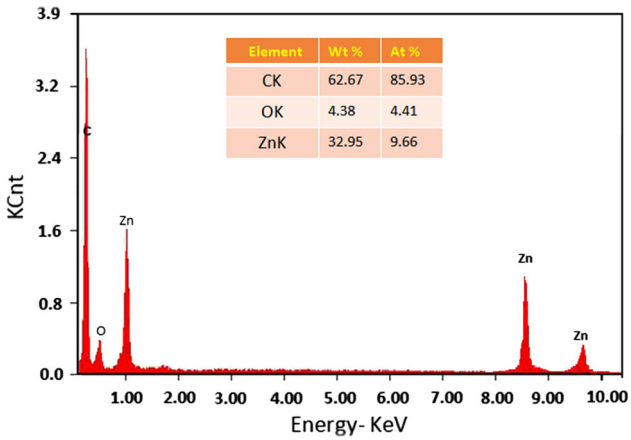

Fig. 5. Microanalysis of expanded graphite (EG).

Fig. 6c and d, respectively. From Fig. 6c, it is reasonably evident that the glazing particles are ZnO, which was established from XRD and EDAX analysis. In Fig. 6d, it is obvious that the ZnO particles have diffused with the graphene layer of the EG surface, which is attributed to the compatibility of ZnO with EG substrates. From Fig. 1 of the prepared EG, it is observed that it has a worm-like appearance. During intercalation of NGFs in the presence of a strong oxidizer, some of the carbon bonds oxidized, leading to the formation of oxygen-carrying functional groups such as carboxylic (COOH) and hydroxyl (–OH) groups.[3] As ZnO nanoparticles are grown over the EG surface, the agglomeration of nanoparticles is obvious, which is observed from Fig. 6e and f. This may be due to a bulky amount of ZnO nanoparticles derived from ZNHH thermal treatment and also may be the physical absorption under ambient conditions (Fig. 2).

The thermal conductivity of the composites was evaluated using the guarded heat flow meter technique, and results are summarized in Table II and plotted in Fig. 7. Pristine epoxy exhibits thermal conductivity of 0.193 W/mK. After incorporation of prepared EG with 5%, 10% and 15% filler fractions, a corresponding increase in thermal conductivity of 4.77, 7.05 and 10 times, respectively, was seen as compared with neat epoxy. The thermal conductivity of the epoxy composites clearly improved, as the thermal conductivity of EG is higher in intensity than that of neat epoxy.[3,20] Moreover, the surface of EG was embedded with ZnO nanoparticles, which was confirmed from XRD and TEM analysis. The thermal conductivity of ZnO is 50 W/mK, which additionally contributes to the thermal conductivity improvement in the epoxy matrix.[21] This intensification of thermal conductivity is by virtue of an effective heat-conductive percolation network created by EG and ZnO nanoparticles throughout the matrix. With the addition of micro-SiC of the same filler fraction as EG, i.e. 5–5 wt.%, 10–10 wt.% and 15–15 wt.% of EG and SiC, the thermal conductivity increased by 1.17, 1.22 and 1.16 times, respectively, relative to simple EG-incorporated epoxy composites. Figure 8 depicts all possible interactions between EG, epoxy and curing agent to facilitate the chemical interaction between filler and matrix. ZnO and SiC are attached to the EG substrates and in physical contact with epoxy resin during the stirring times. The significant enhancement was greater in the case of 10 wt.% addition of micro-SiC in the hybrid composites relative to neat EG addition of 10 wt.%. With regard to two composites carrying 10% filler concentration, EG10-Ep and EG5-S5-Ep, the TC value of EG-10-Ep is 1.26 times that of EG5-S5-Ep. This is because of the van der Waals interaction of ZnO with EG which retains better compatibility than EG and SiC in which higher interface thermal resistance exists.[5] This is attributed to the deprived contact of micro-SiC with the matrix as the result of their irregular polyhedral geometry, making it difficult to form a continuous conductive path at lower filler fractions. Therefore, interfacial thermal Kapitza resistance exists in EG-SiC at 5–5 wt.% filler fraction, and a favorable heat-conducting path is not formed.[22] The overall thermal conductivity value was highest in the case of 15 wt.% of EG and 15 wt.% of the micro-SiC filled composite, which is a 1060.62% increase as compared with neat epoxy. This occurred due to the synergistic compatibility of ZnO nanoparticles with micro-SiC particles. At higher filler fraction, surface-particle interaction between EG and micro-SiC

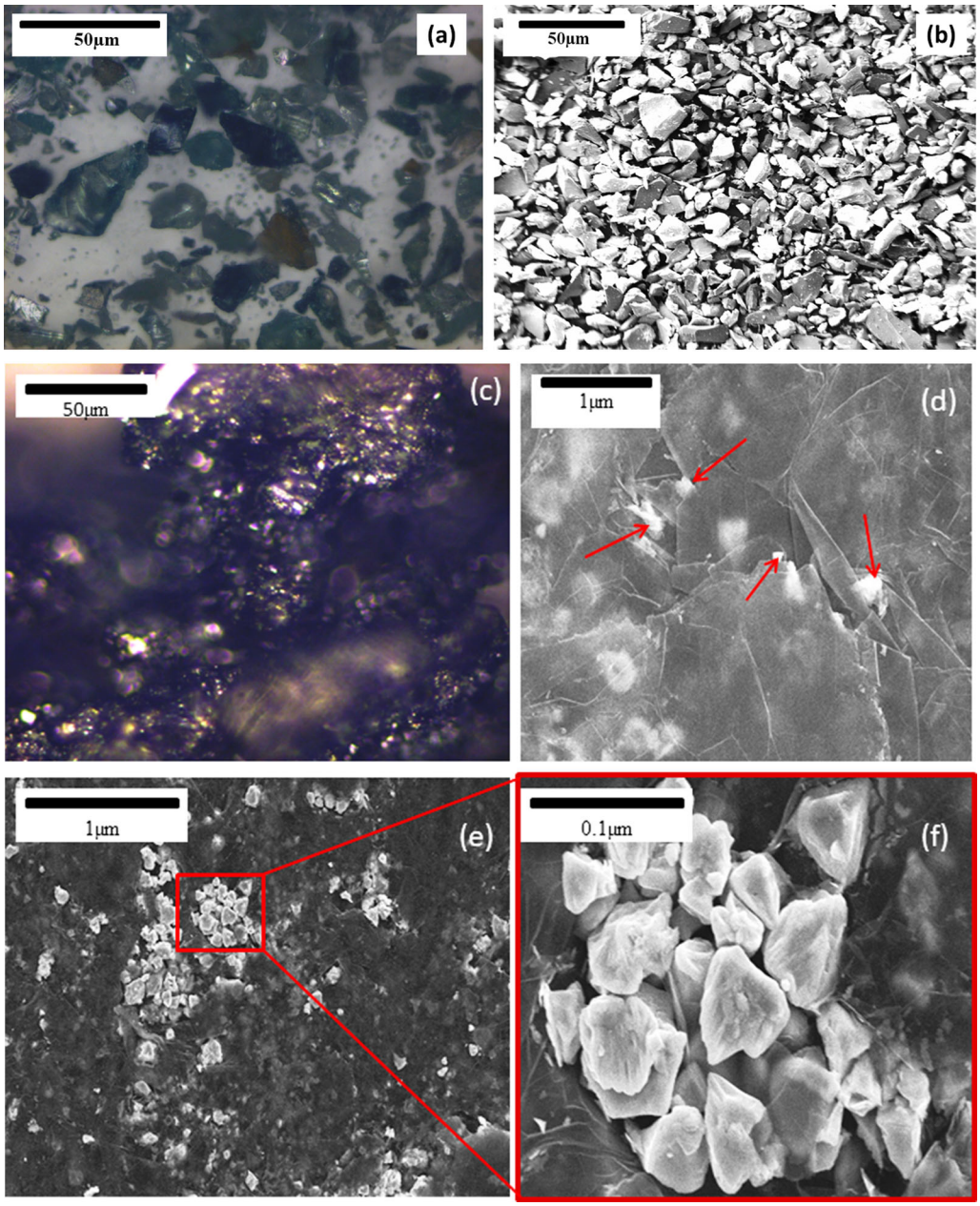

Fig. 6. Optical microscope image of micro-SiC (a) and EG (c), SEM analysis of micro-SiC (b) EG (d), (e) and (f).

Table II. Thermal conductivity, thermal conductivity enhancement with respect to neat epoxy, and thermal resistance of the epoxy composite system

Sample no.	Sample name	Thermal conductivity (W/mK)	Enhancement (%) $\left(\frac{K-K_0}{K_0}\right)$	Absolute thermal resistance (K/W) $\left(\frac{L}{KA}\right)$
1	Neat epoxy (Ep)	0.193 (K_0)	–	2.96
2	EG5-Ep	0.92	376.68	0.623
3	EG5-S5-Ep	1.08	459.58	0.53
4	EG10-Ep	1.36	604.66	0.421
5	EG10-S10-Ep	1.67	765.28	0.343
6	EG15-Ep	1.93	900	0.297
7	EG15-S15-Ep	2.24	1060.62	0.256

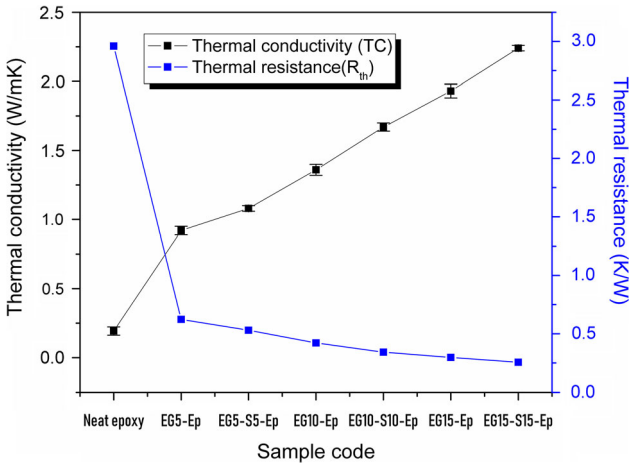

Fig. 7. Thermal conductivity enhancement and absolute thermal resistance reduction of hybrid epoxy composites changes with specified filler fraction of EG and EG-SiC hybrid.

provide better compatibility in the phonon transfer mechanism with each other, reducing filler–filler and filler–matrix resistance. High filler loading and high aspect ratio of the filler contribution played a crucial role in the 11.6-fold improvement in thermal conductivity versus neat epoxy. However, the improvement factor was less when compared with 5–5 wt.% and 10–10 wt.% addition of EG and micro-SiC. The high filler loading of the hybrid filler, the high surface area of EG and the uneven texture of SiC created difficulties in mixing and dispersion inside the matrix, leading to the introduction of microvoids and defects in the final composite (Fig. 6a and b).[14,23,24]

As thermal resistance of materials has a great impact on device cooling, in order to avoid malfunction of an electronic component, the absolute thermal resistance must be evaluated in the design stage. Absolute thermal resistance values of different composites and hybrid composites are listed in Table II. Thermal resistance is the reciprocal of thermal conductance, meaning that less thermal resistance leads to more heat conductivity paths for phonon transfer. The absolute thermal resistance in the case of the prepared neat epoxy sample is higher than another epoxy-based composite, fabricated according to standard ASTM E1530-06, tabulated in Table II. The smallest value of thermal resistance is 0.256 K/W for the highest thermal conductivity sample coded as EG15-S15-Ep. At 5 wt.% EG loading, the resistance value drops sharply and then further decreases gradually to 0.256 K/W. This illustrates that the formation of a conductive path inside the matrix through which phonon transfer takes place is synchronized.[24]

To explore the electrical conductivity of epoxy composites comprising EG and hybrid EG/micro-SiC, the electrical resistance was measured using a four-point potentiometer at a constant voltage. The prime objective for evaluating electrical conductivity of the epoxy composite was to determine the range of the electron conductivity of the material (i.e. insulator or semiconductor). Thus, suitable applications for attaching bare matrices, flexible electronics, ceramic substrates (low-temperature co-fired ceramic; LTCC) and many electronics applications, such as protective encapsulation packaging, can be established.

From Table III, it is seen that with increasing concentration of EG, the electrical resistance of the composite decreases, and consequently electrical conductivity increases. The composite EG15-Ep shows the lowest log of electrical resistivity of 4.98 Ω cm and highest electrical conductivity of 1.048×10^{-3} $(\Omega\ \mathrm{m})^{-1}$ among all the designated composites. As graphite exhibits room temperature electrical conductivity of 3×10^{4} $(\Omega\ \mathrm{m})^{-1}$ to 2×10^{5} $(\Omega\ \mathrm{m})^{-1}$, the EG-filled composites were expected to have greater electrical conductivity. However, the presence of air gaps between the graphitic layer and ZnO nanoparticles on the EG surface reduced the conductivity value from the predicted value. After the addition of equal weights of micro-SiC and EG, the electrical resistivity of the hybrid composites was enhanced, as observed in the EG5-S5-Ep, EG10-S10-Ep and EG15-S15-Ep hybrid composites (Fig. 9a), which was due to the electrical insulating properties of ceramic SiC (10^{-8} $(\Omega\ \mathrm{m})^{-1}$). Additionally, the high bandgap energy of ZnO (3.3–3.6 eV) contributes to the high electrical resistivity of hybrid composites.[25]

According to percolation theory, the composites containing EG as filler have the ability to form clusters of filler inside the matrix. At low filler addition, EG can propagate inside the epoxy in an indiscriminate manner, which creates a continuous path for electron conduction. With increased EG inside the epoxy matrix, the formation of continuous clusters supports the flow of electrons throughout the composites. Hence, near the percolation transition point, i.e. at 12.24 wt.% EG addition of composite, there is a sharp decrease in electrical resistivity, which is evident from Fig. 9a. The percolation threshold (w_C) is determined from the curve fitting of the Sigmoidal-Boltzmann model expressed in Eq. 4.

$$Y = A_2 + \frac{A_1 - A_2}{1 + e^{\left(\frac{x - x_0}{\Delta x}\right)}} \tag{4}$$

where Y is the dependent factor of electrical conductivity at the corresponding independent factor volume fraction x. A_1 and A_2 represent initial and final data of electrical conductivity. Δx is the slope that specifies the gradient of the curve and x_0 related to x-axis value is termed as the percolation threshold point (w_C) when the second-order derivative of Eq. 4 is zero.[26] From Fig. 9b, the electrical conductivity of neat EG loaded composite is illustrated by notifying the percolation threshold point just before 15% EG fraction.

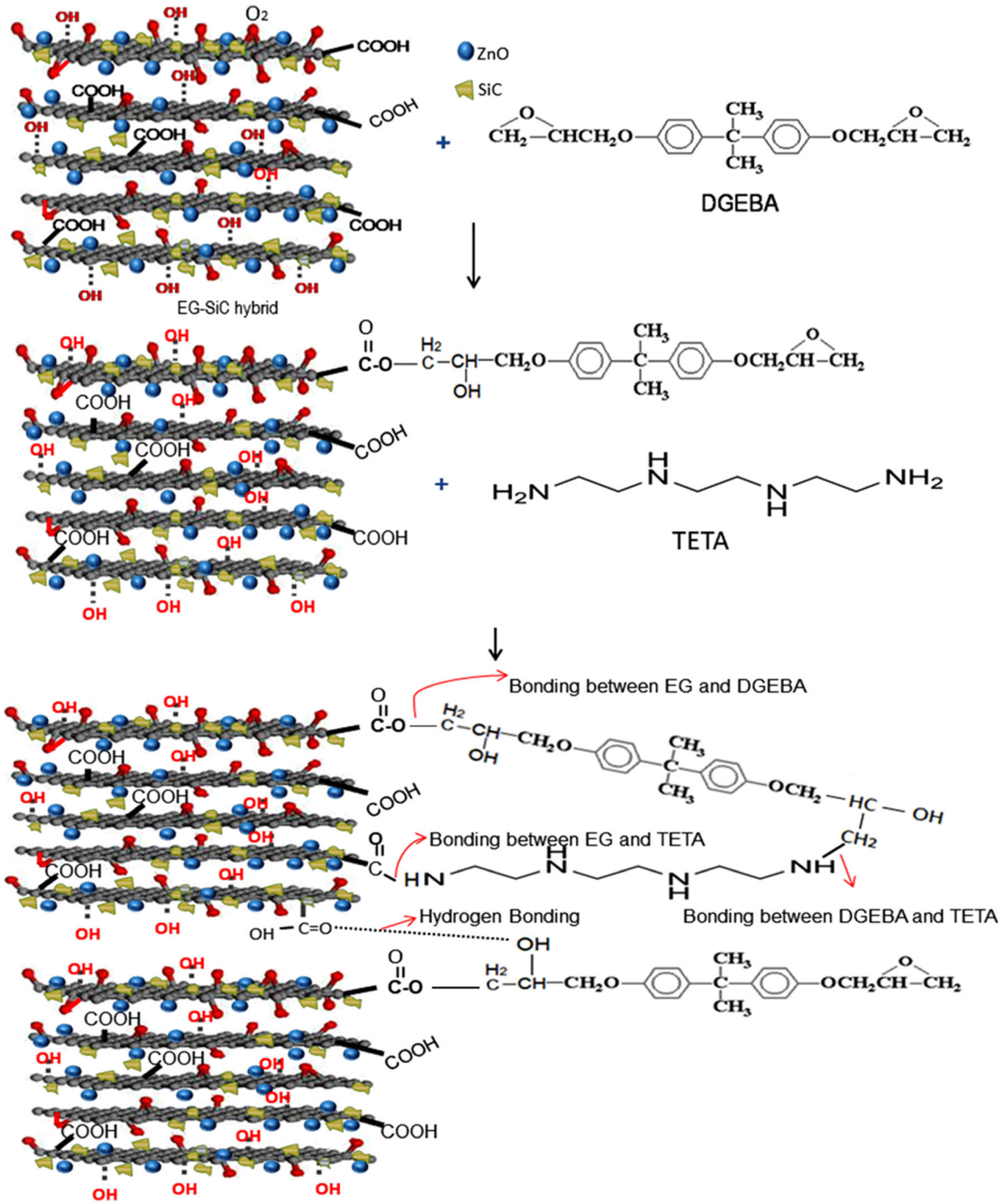

Fig. 8. Schematic illustration for chemical interactions between epoxy, EG, and TETA.

The air gap, ZnO nanoparticles, and SiC are major barrier factors for abasement of electrical conductivity in composites. The composite EG15-Ep is under the range of semiconducting material from insulated epoxy as the electrical conductivity of semiconductors is in the range of 10^{-6}–10^{4} $(\Omega\ m)^{-1}$.[27] However, all other composites described in Table III remain in the insulating range satisfying the criteria of thermally conductive and electrically insulating TIMs for various electronics and microelectronics application where only heat evacuation is the prime concern.

Table IV summarizes the single-lap shear strength and failure mode of the epoxy composite system which banded aluminium metallic sheets. From Table IV it is seen that as the filler content increases, the shear strength increases, but up to the composite EG10-S10-Ep. The shear/peel strength of the epoxy composite system containing various fractions of EG and EG-SiC filler are shown in Fig. 10. The highest result was observed for the sample containing 10 wt.% EG and 10 wt.% micro-SiC which is tuned to 8.21 MPa in which the peel

Table III. Bulk electrical resistivity of epoxy composites containing EG and EG-SiC hybrid filler

Sample no.	Sample code	EG loading (wt.%)	SiC loading (wt.%)	Electrical resistivity (Ω m)	Electrical conductivity $(\Omega\ m)^{-1}$
1	Neat epoxy	0	0	5.32×10^{14}	1.88×10^{-15}
2	EG5-Ep	5	0	8.89×10^{12}	1.1248×10^{-13}
3	EG10-Ep	10	0	5.22×10^{6}	1.915×10^{-7}
4	EG15-Ep	15	0	9.54×10^{2}	1.048×10^{-3}
5	EG5-S5-Ep	5	5	9.15×10^{13}	1.0928×10^{-14}
6	EG10-S10-Ep	10	10	3.65×10^{8}	2.739×10^{-9}
7	EG15-S15-Ep	15	15	9.78×10^{6}	1.022×10^{-7}

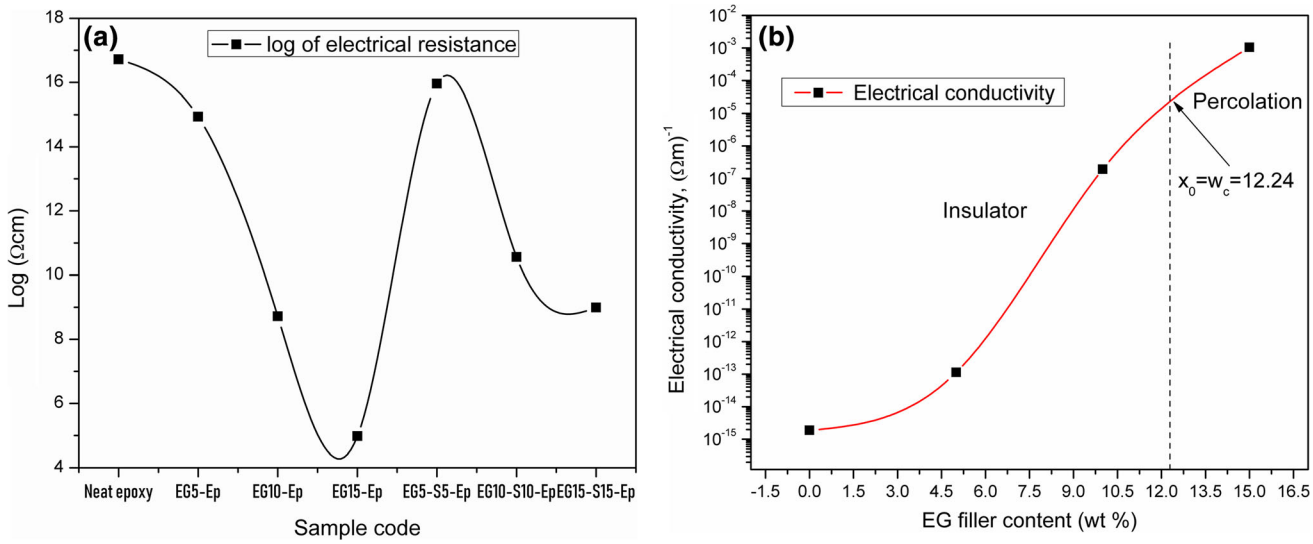

Fig. 9. (a) Dependence of the logarithm of the bulk electrical resistance on the concentration of EG and EG-SiC hybrid filler, (b) Electrical conductivity with respect to EG loading; the percolation threshold (w_c = 12.24 wt.%) is determined by Eq. 4.

Table IV. Joint strength of epoxy and its composite system

Sample No	Sample type	Lap shear strength (MPa)	Types of failure
1	Neat epoxy	4.65 ± 0.31	Interfacial
2	EG5-Ep	6.12 ± 0.39	Interfacial-cohesive
3	EG5-S5-Ep	7.23 ± 0.3	Interfacial-cohesive
4	EG10-Ep	7.86 ± 0.2	Interfacial-cohesive
5	EG10-S10-Ep	8.21 ± 0.4	Interfacial-cohesive
6	EG15-Ep	7.19 ± 0.2	Interfacial-cohesive
7	EG15-S15-Ep	6.32 ± 0.5	Interfacial-cohesive

strength was 1.77 times better than neat epoxy. The enhancement of adhesive bond strength with the filler fraction may be due to the resistance to fracture provided by the fillers with the help of an interfacial crack propagation mechanism. The effective filler–filler interaction and well-dispersed filler in the matrix divert the crack transmission by absorbing the strain energy through well-distributed stress. The filler–matrix deboning would also affect the localized plastic shear yield, and reduce nucleation inside the matrix by absorbing stored strain energy, leading to suppression of crack propagation.[28] Further, with the loading of 15 wt.% of EG and 15–15 wt.% of EG-SiC to the epoxy, the lap shear strength tuned to 7.19 MPa and 6.32 MPa, respectively. This reduction is due to the abundant amount of oxygen/air present between the layers of EG which confine the cohesive strength of adhesive composites as void formation and agglomeration at high filler loading is prevalent. As micro-SiC powder has an uneven texture, the synergistic effect with EG could limit the adhesive bond strength with matrix and metal substrates. This is possibly attributable to an increase in filler

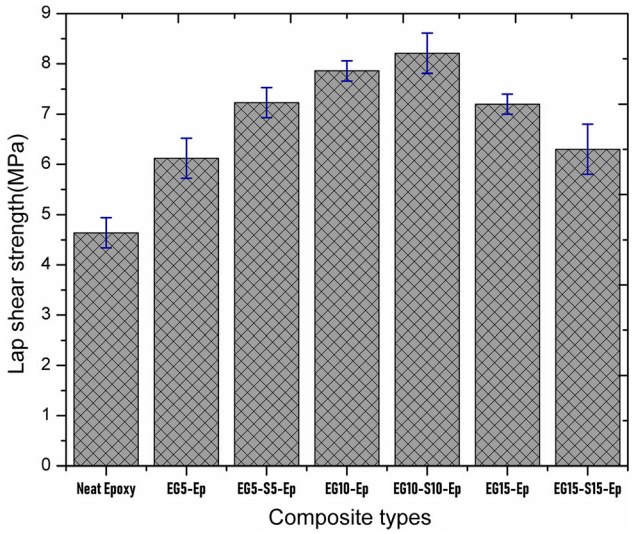

Fig. 10. Lap shear strength of EG and EG-SiC loaded epoxy composites at different filler fractions.

loading to equal to or greater than 15 wt.%, leading to the formation of fault-containing aggregations, and the stress concentration inside the matrix reduced the stress up to 30% with respect to composite EG10-S10-Ep.[24,28,29]

It is important to consider the effects of bond line thickness (BLT) of the adhesive and surface treatment of aluminium substrate on the interfacial bond strength with the adhesive composite and cohesive strength within the adhesive composites. The mechanical roughening of Al substrates leads to the development of oxygen-deficient aluminium oxide (Al_2O_3), which binds with the oxygen existing in epoxide dimer or trimer through electron sharing, leading to better joint strength.[28] The fracture pattern of neat epoxy is usually interfacial (composite-substrates) in nature, as confirmed by Badwe et al.[30] in their work on interfacial failure of copper/epoxy-resin interfaces by applying a pull test method. However, composites containing EG and EG-SiC hybrid up to 30 wt.% exhibited both interfacial and cohesive (composite–composite) failure. This type of failure predicts the crack propagation through the bulk composite and then change-over to the interface which would lead to absorption of more energy to fail. Similar observations have been reported by Kumar et al.[24,31] With the exception of neat epoxy lap joint, the shear strength of all the designed composites entered the commercial range of $\sim$ 6 MPa of TIMs.[32]

Dynamic mechanical analysis is a pioneering technique for measuring the response of a particular material to cyclic deformation as a function of temperature. The strong influence of EG and micro-SiC on epoxy composites is depicted in Fig. 11. The storage modulus (E'), which measures the elastic response or energy-storing capacity of materials relative to a temperature range of 35–165°C, is observed in Fig. 11a. The E' value of neat epoxy is highest with respect to other composites mentioned in Fig. 11a. The composites EG10-Ep and EG15-Ep have 10 wt.% and 15 wt.% EG, and the composites EG10-S10-Ep and EG15-S15-Ep have 10–10 wt.% and 15–15 wt.% EG and SiC, respectively. The decrease in storage modulus under viscoelastic deformation of composites containing higher filler fraction of EG and EG-SiC can be interpreted as the increased tendency towards agglomeration, leading to less energy dissipation in the composite system. Moreover, the porosity of EG generates free volume inside the filler and matrix. As the temperature increases, the polymer chain mobility increases, which leads to a decrease in the storage modulus. Again, it is observed that the composite EG15-S15-Ep containing 30 wt.% of total hybrid filler shows a higher E' value than composites EG10-S10-Ep (20 wt.%) and EG15-Ep (15 wt.%). This is attributed to the restriction of molecular motion of the epoxy chain as hybrid filler loading is increased. A strong shift is observed below the rubbery region as filler loading is increased, which is the reason for lower chain mobility. Above the glassy region, the storage modulus of the composites increases as filler incorporation increases. This may be due to the synergistic compatibility of SiC and ZnO nanoparticles with EG substrates and matrix. Hence, the E' value enhances the range of 75–115°C.[24,33,34]

The glass transition temperature (T_g) of neat epoxy and epoxy composites is illustrated in Fig. 11-b. From Fig. 11b, it is evident that the T_g of neat epoxy is 90°C and improved as filler incorporation increased. The T_g increased to 96°C, 109°C, 108°C and 109°C for the corresponding composite samples EG10-Ep, EG10-S10-Ep, EG15-Ep, and EG15-S15-Ep. The peak height of EG15-S15-Ep was also reduced as compared with EG10-S10-Ep and EG15-Ep because of the effective spreading of filler within sufficiently incorporated epoxy chains in the EG10-S10-Ep and EG15-Ep composites, preventing the dissipation of vibrational motion energy of epoxy chains as the number of physical cross-links increased. The temperature range and tan $\delta > 0.3$ are the key parameters for estimating the damping properties of the composite. The temperature range of neat epoxy was 65–135°C and the resultant damping peak was 0.89. For the EG10-Ep, EG10-S10-Ep, EG15-Ep, and EG15-S15-Ep composite samples, the temperature ranges were 71–140°C, 77–144°C, 79–149°C and 84–152°C, respectively. The respective tan δ peaks were 0.63, 0.65, 0.51 and 0.62. The peak for composite EG15-S15-Ep was higher than that for EG10-S10-Ep. This might be attributable to the introduction of voids and cracks at the time of filler loading, leading to increased viscosity and particle agglomeration. As a consequence, the cross-linking density decreased inside the matrix.[24,33–36]

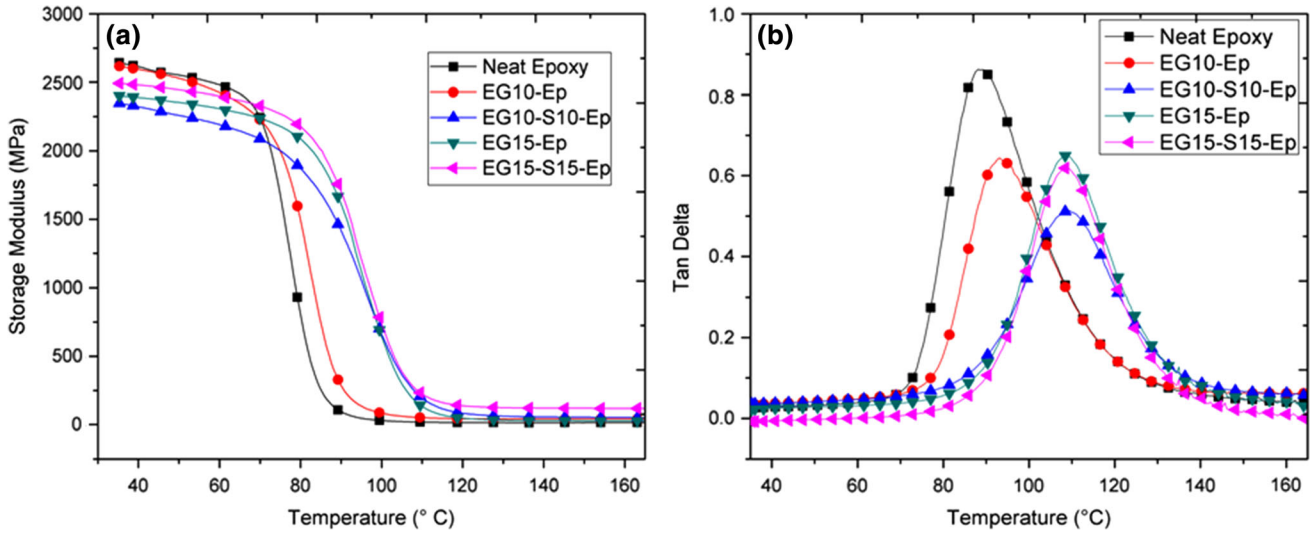

Fig. 11. (a) Storage modulus and (b) damping factor (tan delta) of the epoxy composite system.

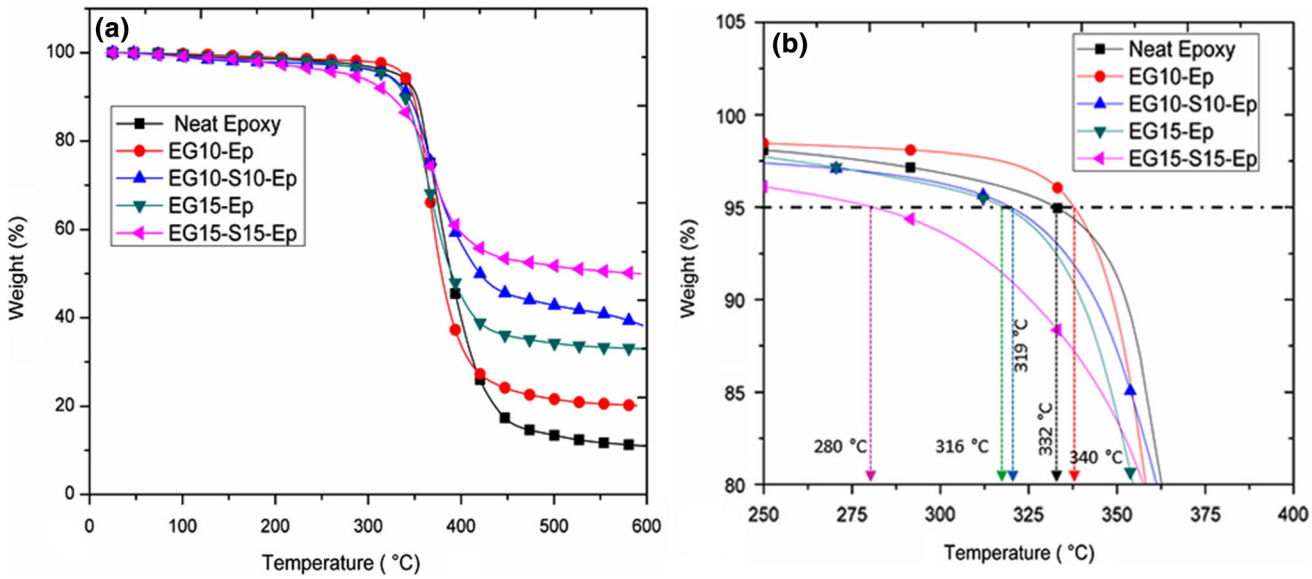

Fig. 12. TGA thermogram of the epoxy composite system (a) and with respect to 5 wt.% loss (b).

To analyze the effect of EG and EG-SiC on the thermal stability of the epoxy composite systems, TGA characterization was carried out in a nitrogen atmosphere, and the curves are presented in Fig. 12. Figure 12b illustrates the start of decomposition considering 5 wt.% loss. The data reveal that the neat epoxy was stable up to 332°C, and the loss was due to the removal of moisture and oligomer decomposition. After the addition of EG, the decomposition temperature shifted to 340°C. Because of the porous nature of EG and the presence of ZnO nanoparticles, the disintegration started at a higher temperature. The significant improvement in thermal stability is also due to the barrier effect of carbon. In the composites EG10-S10-Ep, EG15-Ep and EG15-S15-Ep, the degradation temperature decreased to 319°C, 316°C and 280°C, respectively. This is due to the low wettability of epoxy, leading to non-homogenous dispersion of high amounts of filler. As EG is highly porous and low-density in nature, it can carry moisture and air between graphitic layers, which induces loss as the temperature rises. This can be explained by the physical absorption of moisture on the carbon plane or by the hydrogen bonding of water with the planar structure of carbon. However, at 40 wt.% loss, the neat epoxy showed 380°C, whereas the optimized composite EG15-S15-Ep demonstrated 400°C. The hindering effect of hybrid filler inside the epoxy matrix restricts the polymer

chain mobility towards degradation. From Fig. 12 it is also observed that the residue mass retention is highest in the EG15-S15-Ep hybrid composite. The remaining residue is increased as filler loading increases.[24,28] The corresponding melting points of ZnO and SiC are 1975°C and 2830°C, which prevents the overall degradation of epoxy composites. Therefore, the high residual mass is due to the high amount of filler inside the epoxy matrix. However, the formulated hybrid epoxy composites performed well up to 280°C, and no consequential weight loss was observed up to 280°C. Based on these parameters, this hybrid epoxy composite could be utilized as a packaging material for a high heat generator multifunctional device for long-term application.[37,38]

Figure 13 shows the fracture surface of the EG-epoxy and EG/SiC-epoxy composite systems. The fracture morphology of the EG5-Ep, EG10-Ep, and EG15-Ep composites is shown in Fig. 13a, b and c, respectively. We can see that the porous and fluffy nature of EG inside the epoxy results from its very low density, as also seen in Fig. 2. Two grams of both NGFs and EG were put into a measuring cylinder, and it was found that NGF showed a volume of 3.5 cm^3, whereas EG showed a volume of 40 cm^3. The loose worm-like and intercalated lamellar structure of EG can catalyze to improve the thermal and mechanical properties of composites with minimal incorporation. The wettability of epoxy towards EG is very poor, due to which a patchy dispersion of EG inside epoxy takes place, and consequently numerous holes and gaps between EG and epoxy hinder the thermal conductivity of the composite, as air retains negligible thermal conductivity. The addition of more EG with epoxy increases the number of voids and occurrence of agglomeration. For this reason, researchers try to minimize EG incorporation by looking at the density of filler which affects the processability of the composite, as increased viscosity is a major concern. With the addition of micro-SiC via mechanical mixing through cryomilling, the interlayer distance between EG decreased, and a slight improvement in density occurred by the bombardment of SiC particles inside the shaking mill. The dispersion of the EG-SiC hybrid is more favorable inside the epoxy as compared with mono-filler loading. The fracture morphology of hybrid composites EG5-S5-Ep, EG10-S10-Ep and EG15-S15-Ep is presented in Fig. 13d, e and f, respectively. From these fracture surfaces, it is clear that the void and gap formation has been reduced, and SiC particle distribution is discernable in the yellow circle. The red arrows indicate the holes introduced at the time of composite fabrication. The micro-SiC powder acts as an effective heat-conductive bridge between each EG strand, as demonstrated in Fig. 13f. Thus, the addition of SiC contributes to the development of

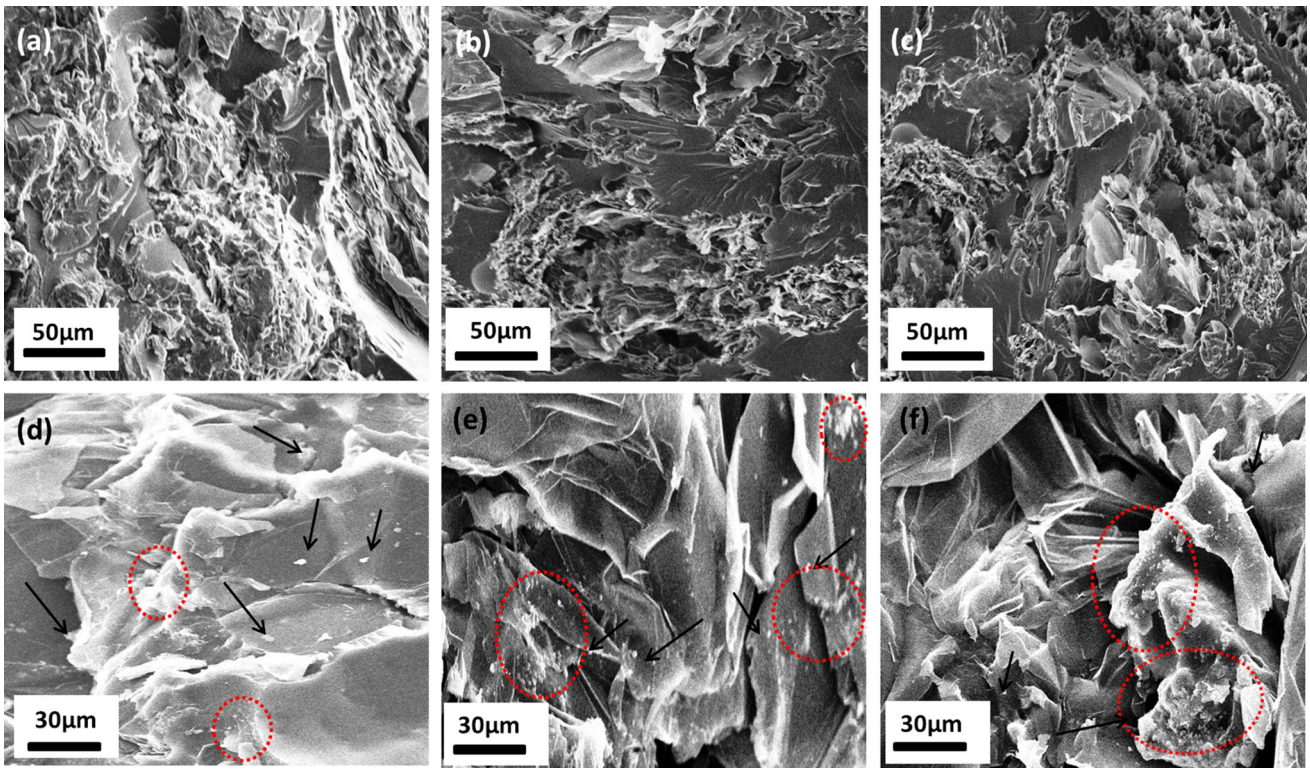

Fig. 13. SEM micrograph of (a) EG5-Ep, (b) EG10-Ep, (c) EG15-Ep, (d) EG5-S5-Ep, (e) EG10-S10-Ep, (f) EG15-S15-Ep.

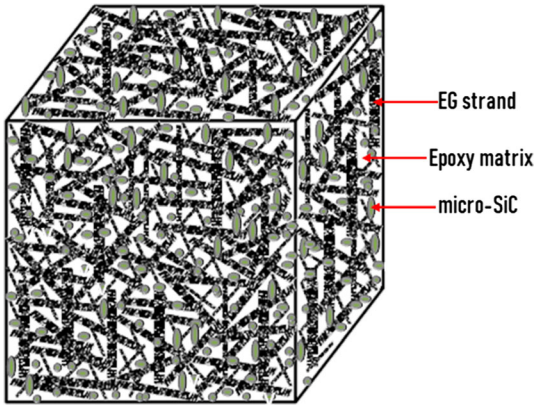

Fig. 14. Schematic heat conductive networks in the epoxy matrix containing EG/micro-SiC hybrid.

an efficient 3D phonon network for heat transfer inside the matrix (Fig. 14). In addition, electrical resistivity is improved with the incorporation of SiC at an equal fraction to EG, as discussed in Fig. 9a.

CONCLUSION

In this study, EG was synthesized from natural graphite flakes using zinc nitrate hexahydrate as an intercalating agent. XRD, TEM, SEM, and EDAX analysis confirmed the formation of an intercalated structure with the attachment of ZnO nanoparticles on the EG surface. Micro-SiC and/or synthesized EG were used to improve the thermal conductivity of DGEBA epoxy. By adding 15 wt.% EG and 15 wt.% SiC to the epoxy resin, the thermal conductivity of the hybrid composite was increased 11.6-fold as compared with unaided epoxy. Lap shear strength, and dynamic mechanical and thermogravimetric analysis validated the prepared hybrid composite with suitable end-use. The effect of ZnO nanoparticles and SiC on the electrical conductivity of the hybrid composites was also noted. As ZnO and SiC are ceramic materials, they demonstrated thermal conductive and electrical insulating properties inside the matrix. As a consequence, the high-thermal-conductivity hybrid composite retains the insulating properties of pristine epoxy. SEM images of the hybrid composites also showed the formation of long-range 3D percolation connectivity through which phonon and electron transfer took place. Taken together, these results establish high-efficiency TIMs as a potential candidate for advanced microelectronics and optoelectronics applications.

ACKNOWLEDGMENTS

This work is supported by the Board of Research in Nuclear Science (BRNS), Department of Atomic Energy (DAE), Govt. of India (project No.39/14/01/2018-BRNS/39001).

REFERENCES

1. L. Zhang, H. Deng, and Q. Fu, *Compos. Commun.* 8, 74 (2018).
2. H. Chen, V. Ginzburg, J. Yang, Y. Yang, W. Liu, Y. Huang, W. Liu, Y. Huang, L. Du, and B. Chen, *Prog. Polym. Sci.* 59, 41 (2016).
3. Z. Wang, R. Qi, J. Wang, and S. Qi, *Ceram. Int.* 41, 13541 (2015).
4. R. Moosaei, M. Sharif, and A. Ramezannezhad, *Polym. Test.* 60, 173 (2017).
5. K. Srinivas and M.S. Bhagyashekar, *J. Miner. Mater. Charact. Eng.* 3, 76 (2015).
6. S.Y. Mun, H.M. Lim, and S.H. Lee, *Mater. Res. Bull.* 97, 19 (2018).
7. A. Yasmin, J.J. Luo, and I.M. Daniel, *Compos. Sci. Technol.* 66, 1182 (2006).
8. B. Román-Manso, Y. Chevillotte, M.I. Osendi, M. Belmonte, and P. Miranzo, *J. Eur. Ceram. Soc.* 36, 3987 (2016).
9. A. W. Weimer, in *Carbide, Nitride and Boride Materials Synthesis and Processing* (Springer, Dordrecht, 1997), p. 79.
10. S. E. Saddow, A. Agarwal, *Advances in Silicon Carbide Processing and Applications* (Artech House, 2004).
11. D. Ding, Y. Shi, Z. Wu, W. Zhou, F. Luo, and J. Chen, *Carbon* 60, 552 (2013).
12. Y. Mu, W. Zhou, C. Wang, F. Luo, D. Zhu, and D. Ding, *Ceram. Int.* 40, 10037 (2014).
13. H. Mei, D. Han, S. Xiao, T. Ji, J. Tang, and L. Cheng, *Carbon* 109, 149 (2016).
14. T. Zhou, X. Wang, X. Liu, and D. Xiong, *Carbon* 48, 1171 (2010).
15. F. Kargar, Z. Barani, R. Salgado, B. Debnath, J.S. Lewis, E. Aytan, K.L. Roger, and A.A. Balandin, *ACS Appl. Mater. Interfaces* 10, 37555 (2018).
16. A. Malas, C.K. Das, A. Das, and G. Heinrich, *Mater. Des.* 39, 410 (2012).
17. Y. Wang, J.E. Panzik, B. Kiefer, and K.K. Lee, *Sci. Rep.* 2, 520 (2012).
18. M.J. Akhtar, M. Ahamed, S. Kumar, M.M. Khan, J. Ahmad, and S.A. Alrokayan, *Int. J. Nanomed.* 7, 845 (2012).
19. C. Rimbu, N. Vrinceanu, G. Broasca, D. Farima, M. Ciocoiu, C. Campagne, M.P. Suchea, and A. Nistor, *Text. Res. J.* 83, 2142 (2013).
20. A. Karaipekli, A. Sarı, and K. Kaygusuz, *Renew. Energy* 32, 2201 (2007).
21. X. Wu, J. Lee, V. Varshney, J.L. Wohlwend, A.K. Roy, and T. Luo, *Sci. Rep.* 6, 22504 (2016).
22. H. Shin, S. Yang, S. Chang, S. Yu, and M. Cho, *Polymer* 54, 1543 (2013).
23. N.K. Mahanta, M.R. Loos, I.M. Zlocozower, and A.R. Abramson, *J. Mater. Res.* 30, 959 (2015).
24. R. Kumar, S.K. Nayak, S. Sahoo, B.P. Panda, S. Mohanty, and S.K. Nayak, *J. Mater. Sci. Mater. Electron.* 29, 16932 (2018).
25. X. Ren, D. Chen, X. Meng, F. Tang, X. Hou, D. Han, and L. Zhang, *J. Colloid Interface Sci.* 334, 183 (2009).
26. M. Rahaman, A. Aldalbahi, P. Govindasami, N. Khanam, S. Bhandari, P. Feng, and T. Altalhi, *Polymers* 9, 527 (2017).
27. L. Melnyk, *Technol. Audit Prod. Reserves* 3, 28 (2017).
28. P.K. Ghosh, S. Halder, M.S. Goyat, and G. Karthik, *J. Adhes.* 89, 55 (2013).
29. S.K. Nayak, S. Mohanty, and S.K. Nayak, *SN Appl. Sci.* 1, 337 (2019).
30. N. Badwe, R. Mahajan, and K. Sieradzki, *Acta Mater.* 103, 512 (2016).
31. R. Kumar, S. Mohanty, and S.K. Nayak, *SN Appl. Sci.* 1, 180 (2019).
32. R. Moriche, S.G. Prolongo, M. Sánchez, A. Jiménez-Suárez, F.J. Chamizo, and A. Ureña, *Int. J. Adhes. Adhes.* 68, 407 (2016).
33. K. Kumar, P.K. Ghosh, and A. Kumar, *Compos. B* 97, 353 (2016).

34. E.V. Kuvardina, L.A. Novokshonova, S.M. Lomakin, S.A. Timan, and I.A. Tchmutin, *J. Appl. Polym. Sci.* 128, 1417 (2013).
35. S. Chandrasekaran, C. Seidel, and K. Schulte, *Eur. Polym. J.* 49, 3878 (2013).
36. H. Im and J. Kim, *Carbon* 50, 5429 (2012).
37. K. Takahashi, A. Yoshikawa, and A. Sandhu, *Wide Bandgap Semiconductors* (Springer Berlin, 2007), p. 239.
38. W. M. Haynes (ed.), *CRC Handbook of Chemistry and Physics*, 92nd edn. (CRC Press, Boca Raton, 2011). ISBN 978-1439855119.